

Persistence weighted Gaussian kernel for topological data analysis

Genki Kusano ^{*} Kenji Fukumizu [†] Yasuaki Hiraoka [‡]

Abstract

Topological data analysis is an emerging mathematical concept for characterizing shapes in multi-scale data. In this field, persistence diagrams are widely used as a descriptor of the input data, and can distinguish robust and noisy topological properties. Nowadays, it is highly desired to develop a statistical framework on persistence diagrams to deal with practical data. This paper proposes a kernel method on persistence diagrams. A theoretical contribution of our method is that the proposed kernel allows one to control the effect of persistence, and, if necessary, noisy topological properties can be discounted in data analysis. Furthermore, the method provides a fast approximation technique. The method is applied into several problems including practical data in physics, and the results show the advantage compared to the existing kernel method on persistence diagrams.

1 Introduction

Recent years have witnessed an increasing interest in utilizing methods of algebraic topology for statistical data analysis. This line of research is called *topological data analysis* (TDA) [3], which has been successfully applied to various problems including information science [4, 10, 12], biology [21, 38], brain science [22, 27, 32], biochemistry [17], and material science [20, 25]. The motivation of this approach is to uncover informative topological properties (e.g., connected component, ring, and cavity) in complex geometric configurations of data, and use them as a description of data.

A key mathematical apparatus in TDA is *persistent homology*, which is an algebraic method for extracting robust topological information from the input data. To illustrate the persistent homology intuitively, let us consider a setting of manifold learning. Assume that data points are generated by a distribution with support on a manifold embedded in a high-dimensional Euclidean space. The aim is to make inference on the topology of the underlying manifold from

^{*}Tohoku University, genksn@gmail.com

[†]The Institute of Statistical Mathematics, fukumizu@ism.ac.jp

[‡]Tohoku University, hiraoka@wpi-aimr.tohoku.ac.jp

finite data points. We represent the data points by the r -balls in a common practice, as employed in constructing an r -neighbor graph for many manifold learning algorithms, and consider a filtration generated by increasing radii, i.e., an increasing sequence of balls (Figure 1). While it is expected that, with an appropriate choice of r , the r -ball model can represent the underlying topological structures of the manifold, it is also known that the result is sensitive to the choice of r . If r is too small, the union consists simply of the disjoint r -balls. On the other hand, if r is too large, the union becomes a contractible space. Persistent homology can consider *all* r simultaneously and provide an algebraic expression of topological properties together with their persistence over r . We give the definition and basic properties of persistent homology in Section 2 (for more details, see [2, 3]).

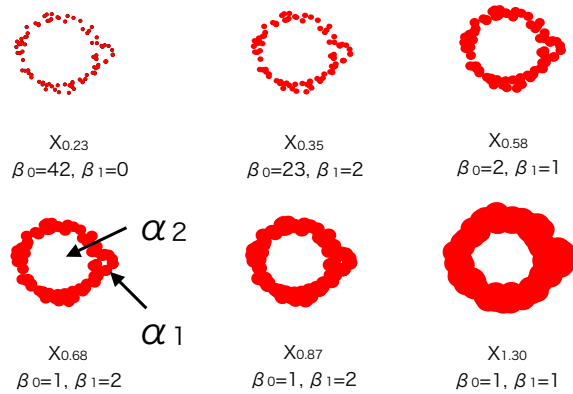


Figure 1: The union X_r of r -balls at points sampled from an annulus with noise. The values β_0 and β_1 are the number of connected components and rings, respectively.

The persistent homology can be visualized in a compact form called a *persistence diagram* $D = \{(b_i, d_i) \in \mathbb{R}^2 \mid i \in I, b_i \leq d_i\}$ [13]. Here, each point (b_i, d_i) , called a generator of the persistent homology, represents a topological property in the input data. Furthermore, the *persistence* $d_i - b_i$ of the generator shows the lifetime of the topological property in the filtration. As an example, for the r -ball model in Figure 1, the rings α_1, α_2 and other tiny ones are expressed as x_1, x_2 , and the other points in the persistence diagram shown in Figure 2. A topological property with large persistence can be regarded as a reliable structure, while that with small persistence (points close to the diagonal) is likely to be noise. In this way, persistence diagrams encode topological and geometric information of data points.

As a useful tool in TDA, persistence diagrams have been studied by many researchers. One of the theoretical concerns is the *stability* of persistence diagrams, asking whether a small change of data causes a small change in the

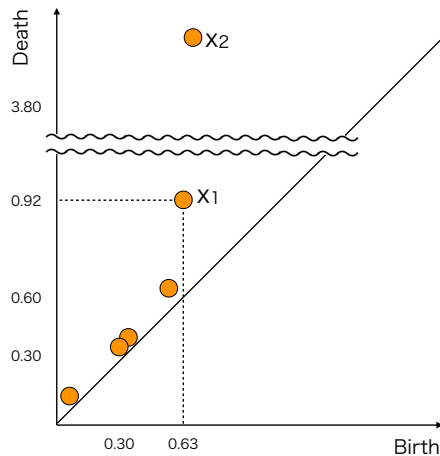


Figure 2: The persistence diagram of the r -ball model in Figure 1. The point x_1 represents the ring α_1 , which is born at $r = 0.63$ and dies at $r = 0.92$. The noisy rings are plotted as the points close to the diagonal.

persistence diagram. It has been proved that this is true for the bottleneck distance [6, 8] (see also Section 2) and the L^p -Wasserstein distance [9] on the persistence diagrams. From statistical perspective, given random data, the paper [15] discusses confidence sets of generators in terms of the distance from the diagonal.

This paper discusses kernel methods for TDA, aiming at developing a framework of statistical data analysis for persistence diagrams. Since a persistence diagram is a point set of variable size, it is not straightforward to apply standard methods of statistical data analysis, which typically treat vectorial data. We introduce a useful class of positive definite kernels on persistence diagrams. The idea of our kernel is based on recent developments of kernel mean [23, 33] in which a probability distribution is embedded as a mean of feature vectors in a Hilbert space. It is also known [34] that more generally, with an appropriate choice of kernels, a signed measure can be uniquely represented by the Bochner integral of the feature vectors with respect to the measure. Since a persistence diagram is regarded as a non-negative measure above the diagonal, it can be embedded into a Hilbert space by the Bochner integral. Once such a vector representation is obtained, we can utilize any kernel methods for persistence diagrams.

In this paper, we propose a *persistence weighted Gaussian kernel* (Section 3) on the space of persistence diagrams. In addition to the Gaussian factor, the kernel has a weight to control the kernel value based on the persistence of generators. This definition reflects the property of persistence diagrams that generators close to the diagonal are likely to be noise and, if necessary, our kernel can discount these generators in data analysis. We also show that the kernel

defines a distance on persistence diagrams and prove stability results with this distance. These stability results ensure the continuity from data to the vector representation of the persistence diagram in a Hilbert space. In Section 4, we demonstrate the proposed method for kernel change point detection [19] and kernel principal component analysis [35] on synthesized data, and experimental/simulation data in physics. The computational results show the effectiveness of our method.

Some works have been already done on the methods for transforming a persistence diagram to a vector: persistence landscape [2], persistent homology rank function [30], and persistence image [7]. In these methods, a transformed vector is a function in a Hilbert space, typically L^p space, and simple summary statistics like means and variances are used as inputs to data analysis, such as principal component analysis and support vector machines. However, these methods do not incorporate the higher-order statistics of persistence diagrams. The most relevant work to our method is studied in [28], where kernel embedding is used to represent persistence diagrams. They use the difference of two Gaussian kernels evaluated at symmetric points with respect to the diagonal so that it vanishes on the diagonal. However, their method cannot explicitly control the persistence, showing the advantage of our method. We give detailed comparisons between our kernel and the one in [28].

2 Background

In this section, we review the concepts of persistence diagrams and kernel methods.

2.1 Persistence diagram

Let $X = \{\mathbf{x}_1, \dots, \mathbf{x}_n\}$ be a finite subset of some metric space (M, d_M) . In practice, X is an input data for some analysis, and we wish to use the topological properties in the analysis. To this aim, let us consider a fattened set $X_r = \bigcup_{i=1}^n B(\mathbf{x}_i; r)$, where $B(\mathbf{x}; r) = \{\mathbf{x}' \in M \mid d_M(\mathbf{x}, \mathbf{x}') \leq r\}$ and r is regarded as a parameter changing resolutions. Then, we use the *homology* $H_q(X_r)$ to describe the topology of X_r . Here, for a topological space S , its q -th homology $H_q(S)$ ($q = 0, 1, \dots$) is defined as a vector space¹ and its dimension $\dim H_q(S)$ measures the number of connected components ($q = 0$), rings ($q = 1$), cavities ($q = 2$), and so on. Because of $X_r \subset X_s$ for $r \leq s$, the set $\mathbb{X} = \{X_r \mid r \geq 0\}$ becomes a filtration² and the inclusion $X_r \hookrightarrow X_s$ induces the linear map $\iota_r^s : H_q(X_r) \rightarrow H_q(X_s)$ in homology. Then, the persistent homology $H_q(\mathbb{X})$ is defined by $\{\iota_r^s : H_q(X_r) \rightarrow H_q(X_s) \mid r \leq s\}$ as a graded module $H_q(\mathbb{X}) = \bigoplus_{r \geq 0} H_q(X_r)$ (see [3] for details).

¹Throughout this paper we use a field coefficient for homology. For accessible introduction to homology, see [24].

²A *filtration* is a family of subsets $\{X_a \mid a \in A\}$ indexed by a partially ordered set A such that $X_a \subset X_b$ for $a \leq b$.

It is known that the persistent homology has a compact expression called the persistence diagram. Let a generator $\alpha_i \in H_q(X_r)$ appear at $r = b_i$ and disappear at $r = d_i$ ($b_i < d_i$) in the filtration. If $\alpha_i \in H_q(X_r)$ does not disappear, we assign $d_i = \infty$. Then, we plot the birth-death pair (b_i, d_i) on $\overline{\mathbb{R}}^2$, where $\overline{\mathbb{R}} = \mathbb{R} \cup \{\infty\}$. By gathering all generators α_i ($i \in I$), we obtain the collection of these pairs $\underline{D}_q(X) = \{(b_i, d_i) \in \overline{\mathbb{R}}^2 \mid i \in I\}$ as a multi-set. The *persistence diagram* $D_q(X)$ is defined by the disjoint union of $\underline{D}_q(X)$ and the diagonal set $\Delta = \{(x, x) \mid x \in \overline{\mathbb{R}}\}$ counted with infinite multiplicity.

For a point $x = (b, d) \in D_q(X)$, the *persistence* $\text{pers}(x) := d - b$ of x is defined by its lifetime. In Figure 2, the persistence of x_2 is the longest and that of x_1 is the second longest. On the other hand, since the other generators have small persistences, they can be seen as noisy rings. In this way, a persistence diagram provides a topological summary of X_r over all r .

There is another type of popular constructions of persistent homology, which supposes a function as an input. Given a function $f : M \rightarrow \mathbb{R}$, a *sub-level set* $F_a = \{\mathbf{x} \in M \mid f(\mathbf{x}) \leq a\}$ defines the persistent homology $H_q(\mathbb{F}) = \bigoplus_{a \in \mathbb{R}} H_q(F_a)$ via the filtration $\mathbb{F} = \{F_a \mid a \in \mathbb{R}\}$ (Figure 3). A function f is said to be *tame* if the rank of homology $H_q(F_a)$ is finite for all $a \in \mathbb{R}$ and the number of homological critical values³ of f is finite. For a tame function $f : M \rightarrow \mathbb{R}$, the persistence diagram of $H_q(\mathbb{F})$ can be defined in a similar way and it is denoted by $D_q(f)$ for short. Note that, for a finite set $X = \{\mathbf{x}_1, \dots, \mathbf{x}_n\}$ of $M \subset \mathbb{R}^d$ and the function $f_X : M \rightarrow \mathbb{R}$ defined by $f_X(\mathbf{x}) = \min_{\mathbf{x}_i \in X} d_M(\mathbf{x}, \mathbf{x}_i)$, f_X is tame and the persistence diagram $D_q(f_X)$ of the sub-level set is the same as $D_q(X)$.

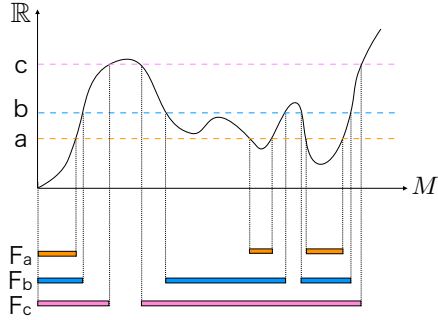


Figure 3: A filtration $\mathbb{F} = \{F_a \mid a \in \mathbb{R}\}$ of sub-level sets.

We measure the distance between two persistence diagrams D and E by the *bottleneck distance*

$$d_B(D, E) := \inf_{\gamma} \sup_{x \in D} \|x - \gamma(x)\|_{\infty},$$

³A *homological critical value* of f is the number $a \in \mathbb{R}$ such that the linear map $H_q(F_{a-\varepsilon}) \rightarrow H_q(F_{a+\varepsilon})$ is not isomorphic for any $\varepsilon > 0$.

where γ ranges over all multi-bijections⁴ from D to E . Note that the cardinalities of D and E are equal by considering diagonal points with infinite multiplicity.

A persistence diagram D is said to be *finite* if \underline{D} is a finite set. It is known that if X is a finite set [6] or f is tame [8], the persistence diagram $D_q(X)$ or $D_q(f)$ is finite, respectively. In this paper, all persistence diagrams are assumed to be finite.

2.2 Stability with respect to d_B

It often happens that data obtained from measurements includes some noise, and thus its topology may be different from that of underlying geometric structure. In such a case, it is desired that the persistence diagrams are stable under perturbation of data.

When the input is given by a function, the stability of the persistence diagram is shown in [8]. Here, we measure the difference between two functions $f, g : M \rightarrow \mathbb{R}$ by $\|f - g\|_\infty = \sup_{\mathbf{x} \in M} |f(\mathbf{x}) - g(\mathbf{x})|$.

Proposition 2.1 (Cohen-Steiner et al. [8]). *Let M be a triangulable compact metric space with continuous tame functions $f, g : M \rightarrow \mathbb{R}$. Then the persistence diagrams satisfy*

$$d_B(D_q(f), D_q(g)) < \|f - g\|_\infty.$$

For finite subsets X and Y of M , $\|f_X - f_Y\|_\infty$ is nothing but the Hausdorff distance $d_H(X, Y)$ given by

$$\max \left\{ \sup_{\mathbf{x} \in X} \inf_{\mathbf{y} \in Y} d_M(\mathbf{x}, \mathbf{y}), \sup_{\mathbf{y} \in Y} \inf_{\mathbf{x} \in X} d_M(\mathbf{x}, \mathbf{y}) \right\}.$$

Hence, we also have the following (for more general setting, see [6]).

Proposition 2.2. *Let X and Y be finite subsets of a metric space (M, d_M) . Then the persistence diagrams satisfy*

$$d_B(D_q(X), D_q(Y)) < d_H(X, Y).$$

Using Proposition 2.2, let us explain a geometric intuition of the stability of persistence diagrams. Assume that X is the true location of points and Y is a data obtained from skewed measurement with $\varepsilon = d_H(X, Y)$ (Figure 4). If there is a point $(b, d) \in D_q(Y)$, then we can automatically conclude that there is at least one generator in X which is born in $(b - \varepsilon, b + \varepsilon)$ and dies in $(d - \varepsilon, d + \varepsilon)$ (Figure 4). Thus the stability guarantees the similarity of two persistence diagrams, and hence allows us to study some features in one persistence diagram by another.

⁴A multi-bijection is a bijective map between two multi-sets counted with their multiplicity.

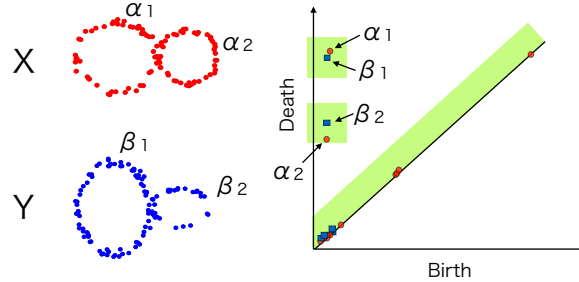


Figure 4: Two data X and Y (left) and their persistence diagrams (right). The green region is an ε -neighborhood of $D_q(Y)$.

2.3 Kernel methods for representing signed measures

Let Ω be a set and $k : \Omega \times \Omega \rightarrow \mathbb{R}$ be a *positive definite kernel* on Ω , i.e., k is symmetric, and for any number of points x_1, \dots, x_n in Ω , the Gram matrix $(k(x_i, x_j))_{i,j=1,\dots,n}$ is nonnegative definite. It is well known that the Gaussian kernel $k_G(x, y) = e^{-\frac{\|x-y\|^2}{2\sigma^2}}$, ($\sigma > 0$) is an example of positive definite kernels on \mathbb{R}^d , where $\|\cdot\|$ is the L^2 -norm of \mathbb{R}^d . It is also known that every positive definite kernel k on Ω is uniquely associated with a reproducing kernel Hilbert space (RKHS), for which k serves as a reproducing kernel, i.e., $\langle f, k(\cdot, x) \rangle_{\mathcal{H}_k} = f(x)$ for each $x \in \Omega$ and $f \in \mathcal{H}_k$. There are many works using positive definite kernels for data analysis; they are called kernel methods (see [31] as a reference).

We use a positive definite kernel to represent persistence diagrams by following the idea of the kernel mean embedding of distributions [33, 34]. Let Ω be a measurable space, $M_b(\Omega)$ be the space of all finite signed Radon measures on Ω , and k be a bounded measurable kernel on Ω . Then we define a mapping from $M_b(\Omega)$ to \mathcal{H}_k by

$$E_k : M_b(\Omega) \rightarrow \mathcal{H}_k, \quad \mu \mapsto \int k(\cdot, x) d\mu(x). \quad (1)$$

The integral should be understood as the Bochner integral [11], which exists when $\int \|k(\cdot, x)\|_{\mathcal{H}_k} d\mu(x)$ is finite. From the boundedness of k and the finiteness of μ , the norm $\|k(\cdot, x)\|_{\mathcal{H}_k} = \sqrt{k(x, x)}$ is integrable.

For a locally compact Hausdorff (LCH) space Ω , let $C_0(\Omega)$ denote the space of continuous functions vanishing at infinity⁵. A kernel k on Ω is said to be C_0 -kernel if $k(x, x)$ is of $C_0(\Omega)$ as a function of x . If k is C_0 -kernel, the associated RKHS \mathcal{H}_k is a subspace of $C_0(\Omega)$. A C_0 -kernel k is called C_0 -universal if \mathcal{H}_k is dense in $C_0(\Omega)$. It is known that the Gaussian kernel k_G is C_0 -universal on \mathbb{R}^d [34]. With C_0 -universal kernel, the mapping E_k defines an injection from $M_b(\Omega)$

⁵A function f is said to vanish at infinity if for any $\varepsilon > 0$ there is a compact set $K \subset \Omega$ such that $\sup_{x \in K^c} |f(x)| \leq \varepsilon$.

to \mathcal{H}_k . Then, from the injectivity, the Bochner integral introduces a distance on $M_b(\Omega)$:

Proposition 2.3 (Sriperumbudur et al. [34]). *If k is C_0 -universal,*

$$d_k(\mu, \nu) = \|E_k(\mu) - E_k(\nu)\|_{\mathcal{H}_k}$$

defines a distance on $M_b(\Omega)$.

3 Kernel on persistence diagrams

In this section, we propose a kernel specializing in a persistence diagram. The kernel enables us to apply any kernel methods to persistence diagrams and defines a distance on persistence diagrams. We also discuss the stability properties with respect to the distance.

3.1 Persistence weighted Gaussian kernel

A finite persistence diagram D can be seen as a sum of Dirac delta measures $\mu_D := \sum_{x \in D} \delta_x$. More generally, we can treat D as an weighted measure $\mu_D^w := \sum_{x \in D} w(x) \delta_x$ with an appropriate weight $w(x) \in \mathbb{R}$ for each generator $x \in D$ (Figure 5). In later application, w is chosen so that we can control the effect of persistence.

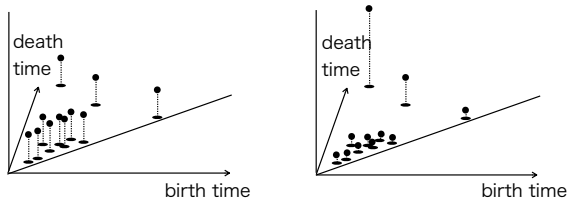


Figure 5: Comparison between μ_D (left) and μ_D^w (right).

As mentioned in Section 2.3, by a positive definite kernel k on \mathbb{R}^2 , the finite signed Radon measure μ_D^w can be transformed into an element of RKHS \mathcal{H}_k via $\mu_D^w \mapsto E_k(\mu_D^w)$. Moreover, if k is C_0 -universal, E_k is injective, and hence there is no loss of information about persistence diagrams. In addition, from Proposition 2.3, $d_k^w(D, E) := \|E_k(\mu_D^w) - E_k(\mu_E^w)\|_{\mathcal{H}_k}$ defines a distance on the set of finite persistence diagrams. In this case, $d_k^w(D, E)$ has the following expansion which

is easy to compute:

$$\begin{aligned} d_k^w(D, E)^2 &= \sum_{x \in \underline{D}} \sum_{x' \in \underline{D}} w(x)w(x')k(x, x') \\ &\quad + \sum_{y \in \underline{E}} \sum_{y' \in \underline{E}} w(y)w(y')k(y, y') \\ &\quad - 2 \sum_{x \in \underline{D}} \sum_{y \in \underline{E}} w(x)w(y)k(x, y). \end{aligned}$$

In this paper, we choose the Gaussian kernel $k_G(x, y) = e^{-\frac{\|x-y\|^2}{2\sigma^2}}$ ($\sigma > 0$) as a C_0 -universal kernel and $w(x) = \arctan(C\text{pers}(x)^p)$ ($C, p > 0$) as an weight function. The reasons of these choices are followings: (i) $w : \mathbb{R}^2 \rightarrow \mathbb{R}$ satisfies $\mu_D^w \in M_b(\mathbb{R}^2)$, (ii) w is an increasing function with respect to persistence so that a noisy (resp. characteristic) generator x corresponds to small (resp. large) value $w(x)$, (iii) parameters C and p can control the weight of generators, (iv) stability properties with respect to $d_{k_G}^w$ hold (Section 3.2).

Following [23], we make a nonlinear kernel on persistence diagrams such as

$$K_{PWG}(D, E) = \exp\left(-\frac{d_{k_G}^w(D, E)^2}{2\tau^2}\right), \quad (2)$$

where τ is a positive parameter. We call K_{PWG} a *persistence weighted Gaussian kernel* (PWGK for short). Although we can also consider a linear kernel

$$K_L(D, E) = \langle E_{k_G}(\mu_D^w), E_{k_G}(\mu_E^w) \rangle_{\mathcal{H}_{k_G}} = \sum_{x \in \underline{D}} \sum_{y \in \underline{E}} w(x)w(y)k_G(x, y),$$

we choose the PWGK as a kernel on persistence diagrams, in this paper, because advantages of using nonlinear kernels are demonstrated in [23], where nonlinear kernels show better performance for classification tasks.

3.2 Stability with respect to $d_{k_G}^w$

Given an input data, we have vectorized its persistence diagram D as an element of RKHS $E_{k_G}(\mu_D^w)$. By the norm $\|\cdot\|_{\mathcal{H}_{k_G}}$, we can measure the distance between two persistence diagrams D, E such as $d_{k_G}^w(D, E) = \|E_{k_G}(\mu_D^w) - E_{k_G}(\mu_E^w)\|_{\mathcal{H}_{k_G}}$. If two input data are similar to each other under an appropriate setting, the following theorems guarantee that the distance $d_{k_G}^w$ between these persistence diagrams is small (see Appendix for proofs). That is, a small change of input data has little effect on the expression of RKHS and the results of kernel methods.

Theorem 3.1. *Let M be a triangulable compact subspace in \mathbb{R}^d , $p > d + 1$ and $f, g : M \rightarrow \mathbb{R}$ be tame Lipschitz functions. Then*

$$d_{k_G}^w(D_q(f), D_q(g)) < L(f, g; C, p, \sigma) \|f - g\|_\infty,$$

where $L(f, g; C, p, \sigma)$ is a constant depending on f, g, C, p, σ .

In the case of finite sets $X, Y \subset \mathbb{R}^d$, by setting $f = f_X$ and $g = f_Y$, we have the following:

Theorem 3.2. *Let M be a compact subset in \mathbb{R}^d , $X, Y \subset M$ be finite subsets and $p > d + 1$. Then*

$$d_{k_G}^w(D_q(X), D_q(Y)) < L(M, d; C, p, \sigma) d_H(X, Y),$$

where $L(M, d; C, p, \sigma)$ is a constant depending on M, d, C, p, σ .

Let $\mathcal{P}_{\text{finite}}(M)$ be the set of finite subsets in a compact subset $M \subset \mathbb{R}^d$. Since the constant $L(M, d; C, p, \sigma)$ is independent of X and Y , we can conclude that the map

$$\mathcal{P}_{\text{finite}}(M) \rightarrow \mathcal{H}_{k_G}, \quad X \mapsto E_{k_G} \left(\mu_{D_q(X)}^w \right)$$

is Lipschitz continuous.

3.3 Calculation of Gram matrix

From now on, we use the symbol D, E , etc. for persistence diagrams without specifying the dimension of homology, and subscripts express indices of diagrams. Let $\mathcal{D} = \{D_\ell \mid \ell = 1, \dots, n\}$ be a collection of persistence diagrams. In many practical applications, the number of points in a persistence diagram can be large. If the persistence diagrams contain at most m elements, then each element of the Gram matrix $(K_{PWG}(D_i, D_j))_{i,j=1,\dots,n}$ involves $O(m^2)$ evaluation of $e^{-\frac{\|x-y\|^2}{2\sigma^2}}$, resulting the complexity $O(m^2 n^2)$ for obtaining the Gram matrix. Hence, reducing computational cost with respect to m is an important issue.

We solve this computational issue by using the random kitchen sink method [29]. To be more precise, let z_1, \dots, z_M be random variables from the 2-dimensional normal distribution $N((0, 0), \sigma^{-2}I)$ where I is the identity matrix.

This method approximates $e^{-\frac{\|x-y\|^2}{2\sigma^2}}$ by $\frac{1}{M} \sum_{a=1}^M e^{\sqrt{-1}z_a x} (e^{\sqrt{-1}z_a y})^*$, where $*$ denotes the complex conjugation. Then, $\sum_{x \in \underline{D}_i} \sum_{y \in \underline{D}_j} w(x)w(y)k_G(x, y)$ is approximated by $\frac{1}{M} \sum_{a=1}^M B_i^a (B_j^a)^*$, where $B_\ell^a = \sum_{x \in \underline{D}_\ell} w(x) e^{\sqrt{-1}z_a x}$. As a result, the computational complexity of the approximated Gram matrix is $O(mnM + n^2M)$. In the computations of this paper, we set $M = 1000$.

We note that the approximation by the random kitchen sink method can be sensitive to the choice of σ . If σ is much smaller than $\|x - y\|$, the relative error can be large. For example, in the case of $x = (1, 2), y = (1, 2.1)$ and $\sigma = 0.01$, $e^{-\frac{\|x-y\|^2}{2\sigma^2}}$ is about 10^{-22} while the approximated value is about 10^{-3} . As a whole, these m^2 errors may cause a critical error to the approximation. Moreover, if σ is largely deviated from the ensemble $\|x - y\|$ for $x \in \underline{D}_i, y \in \underline{D}_j$, then most values $e^{-\frac{\|x-y\|^2}{2\sigma^2}}$ become close to 0 or 1.

In order to obtain a good approximation and extract meaningful values, we follow the heuristics proposed in [18]. We set σ to be close to many $\|x - y\|$ by $\sigma = \text{median}\{\sigma(D_\ell) \mid \ell = 1, \dots, n\}$, where $\sigma(D) = \text{median}\{\|x_i - x_j\| \mid x_i, x_j \in$

\underline{D} , $i < j$. For the parameter C , we also set $C = (\text{median}\{\text{pers}(D_\ell) \mid \ell = 1, \dots, n\})^{-p}$, where $\text{pers}(D) = \text{median}\{\text{pers}(x_i) \mid x_i \in \underline{D}\}$. Similarly, τ is defined by $\text{median}\{a_{k_G}^w(D_i, D_j) \mid 1 \leq i < j \leq n\}$. In this paper, since all points of data are in \mathbb{R}^3 , we set $p = 5$ by following the assumption $p > d + 1$ in Theorem 3.2.

4 Experiments

We demonstrate the effectiveness of the PWGK using synthesized and real data. Among other kernel methods, we show change point detection with kernel Fisher discriminant ratio [19] (KFDR) and kernel principal component analysis [35] (KPCA).

For a collection $\mathcal{D} = \{D_\ell \mid \ell = 1, \dots, n\}$ of persistence diagrams, we use the *kernel Fisher discriminant ratio* $\text{KFDR}_{n,\ell,\gamma}(\mathcal{D})$ (see [19] for the definition) as a statistical quantity for the kernel based change point detection. Here, we set $\gamma = 10^{-3}$ in this paper, and the index ℓ achieving the maximum of $\text{KFDR}_{n,\ell,\gamma}(\mathcal{D})$ corresponds to the estimated change point. The KFDR is calculated by the Gram matrix $(K(D_i, D_j))_{i,j=1,\dots,n}$.

In this section, all persistence diagrams are computed by CGAL [5] and PHAT [26].

4.1 Comparison to the persistence scale space kernel

The most relevant to the PWGK is the *persistence scale space kernel* [28] (PSSK for short) K_{PSS} , which is defined by:

$$\begin{aligned} K_{PSS}(D, E) &= \langle \Phi_t(D), \Phi_t(E) \rangle_{L^2(\Omega)} \\ &= \frac{1}{8\pi t} \sum_{x \in \underline{D}} \sum_{y \in \underline{E}} e^{-\frac{\|x-y\|^2}{8t}} - e^{-\frac{\|x-\bar{y}\|^2}{8t}}, \end{aligned}$$

where $\Phi_t(D) = \frac{1}{4\pi t} \sum_{y \in \underline{D}} e^{-\frac{\|x-y\|^2}{4t}} - e^{-\frac{\|x-\bar{y}\|^2}{4t}}$, $\Omega = \{(x^1, x^2) \in \mathbb{R}^2 \mid x^1 \leq x^2\}$, and $\bar{y} = (y^2, y^1)$ for $y = (y^1, y^2)$.

Note that the PSSK also takes zero on the diagonal. In spite of this similarity between the PWGK and the PSSK, the former has several advantages over the latter. (i) The map $D \mapsto E_{k_G}(\mu_D^w) \in \mathcal{H}_{k_G}$ used in the PWGK can control the effect of the persistence by changing parameters C and p , while the map $D \mapsto \Phi_t(D) \in L^2(\Omega)$ cannot explicitly control the persistence. Thus, the PWGK has more flexibility on the extent to disregard noisy generators. (ii) The approximation by the random kitchen sink method is not possible for the PSSK. It is not shift-invariant in total, and thus Bochner's theorem cannot be applied. If we apply the approximation to the two terms $e^{-\frac{\|x-y\|^2}{8t}}$ and $e^{-\frac{\|x-\bar{y}\|^2}{8t}}$ separately, the choice of the bandwidth parameter t would be difficult for a good approximation of K_{PSS} . For instance, given $x = (1, 2)$ and $y = (1, 2.1)$, we have $\|x - y\| = 0.1$ and $\|x - \bar{y}\| \approx 1.48$, and hence t cannot be chosen appropriately.

(iii) We also note that in [28], only the linear kernel is combined to the PSSK as a kernel on the RKHS, while our proposed method considers the Gaussian kernel on the RKHS.

In light of (ii) discussed above, we calculate the Gram matrix of the PSSK without approximation in this paper. The computational time of the PSSK thus takes $O(m^2n^2)$.

With respect to the parameter t , since $e^{-\frac{\|x-y\|^2}{8t}}$ is only used to vanish the value of the feature map $\Phi_t(D)$ on the diagonal, we set $t = \sigma^2$ by using the same σ defined in Section 3.3.

4.2 Synthesized data

To compare the performance between the PWGK and the PSSK, we calculate the change point determined by the KFDR for both methods. An underlying space $T_{R,r}$ that we use here is given by

$$\begin{aligned}x &= R \cos(s) + r \cos(t) \cos(s), \\y &= R \sin(s) + r \cos(t) \sin(s), \\z &= r \sin(t),\end{aligned}$$

where $s \in [-\pi, \pi)$, and $t \in [-\pi, \pi)$ for $R \geq r$ or $t \in [-\pi + \arccos(\frac{R}{r}), \pi - \arccos(\frac{R}{r})$ for $R < r$. The space $T_{R,r}$ is a torus for $R > r$ and a sphere S^2 for $R < r$ (Figure 6). When we fix $r > 0$ and vary R , the point where $T_{R,r}$ changes from spheres to tori is $R = r$.



Figure 6: Sampling from $T_{R,r}$ for $R < r$ (left, sphere), $R = r$ (center), and $R > r$ (right, torus).

In this example, 1000 points are uniformly sampled from $T_{R,2}$ for each $R = R_\ell$, where $R_\ell = 1.5 + 0.025\ell$, $\ell = 1, \dots, 40$. Then we compute the 2-dimensional persistence diagrams of them. We estimate the change point by the KFDR with respect to the PWGK and the PSSK, where the parameters are defined in Section 3.3 and Section 4.1. We repeat this procedure 50 times. The means of the estimated change points for the PWGK and the PSSK are 20.14 and 20.46. It shows that both methods capture the points close to the true change point $\ell = 20$. The mean absolute errors for the PWGK and the PSSK are 1.58 (STD 1.55) and 2.02 (STD 2.53), respectively. It implies the advantage of the PWGK over the PSSK in the accuracy of detecting the change point.

4.3 Analysis of granular system

We apply the PWGK to persistence diagrams made from experimental data in a granular packing system [16]. In this example, a partially crystalized packing with 150,000 monosized beads (diameter = 1mm, polydispersity = 0.025mm) is obtained by experiment. One of the fundamental interests in the study of granular packings is to understand the transition from random packings to crystalized packings. In particular, the maximum packing density ϕ_* that random packings can attain is still a controversial issue (e.g., see [37]). Here, we apply the change point analysis to statistically detect ϕ_* . Furthermore, we compare the PWGK and the PSSK in terms of computational cost.

We divide the original full system into 35 cubical subsets containing approximately 4000 beads, which are offered from the authors of the paper [16]. The packing densities of the subsets range from $\phi = 0.590$ to $\phi = 0.730$. In the work [36], the authors computed a persistence diagram for each subset by taking the beads configuration as a finite subset in \mathbb{R}^3 , and found that the persistence diagrams characterize different configurations in random packings (small ϕ) and crystalized packings (large ϕ). Hence, it is expected that the change point analysis applied on these persistence diagrams can detect the maximum packing density ϕ_* as a transition from the random to crystalized packings.

Let $\{D_\ell \mid \ell = 1, \dots, 35\}$ be a collection of the persistence diagrams sorted by the increasing order of the packing density. In Figure 7, the both graphs detect $\ell = 12$ as the maximum of the KFDR. This result statistically indicates that the maximum packing density ϕ_* exists in the interval $[0.604, 0.653]$ and supports the traditional observation $\phi_* \approx 0.636$ [1].

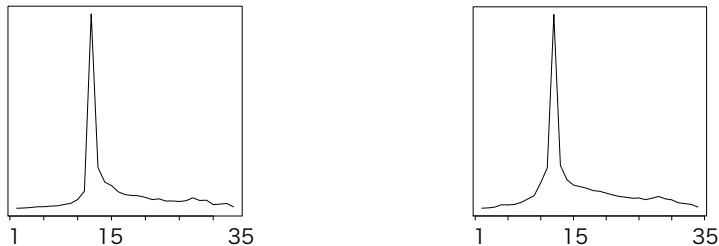


Figure 7: The KFDR graphs of the PWGK (left) and the PSSK (right).

We emphasize that the computational time of the Gram matrix of the PWGK is much faster than that of the PSSK (Figure 8). In the same setting of the computer⁶, the PWGK takes about 20 seconds, while the PSSK takes about 35 hours.

We also apply KPCA to the same collection of the 35 persistence diagrams. Figure 9 shows the 2-dimensional KPCA plots in red for random packing and in blue for crystalized packing have clear two cluster structure corresponding to the two phases.

⁶MacBook Pro, 2.6 GHz Intel Core i5, 8 GB 1600 MHz DDR3



Figure 8: The Gram matrix of the PWGK (left) and that of the PSSK (right). Each matrix is expressed as a heat map; that is, strong red point and light yellow point represent a high value and a low value, respectively.



Figure 9: The KPCA plots of the PWGK (left) and the PSSK (right).

4.4 Analysis of SiO_2

In this example, we study the glass transition temperature of the material SiO_2 . When we rapidly cool down the liquid state of SiO_2 , it avoids the usual crystallization and changes into a glass state. Understanding the glass transition is an important issue in the current physics. For estimating the glass transition temperature by molecular dynamics simulations, we first prepare atomic configurations of SiO_2 for a certain range of temperatures, and then draw the temperature-enthalpy graph. The graph is convex sandwiched by two lines corresponding to the liquid and glass states. The glass transition temperature is usually estimated in an interval where the second derivative of the graph does not vanish (e.g., see [14]). However, since the slopes of the two lines are close to each other, determining the interval is a delicate problem and it is desired to make a mathematical framework to detect the glass transition temperature.

Let $\{D_\ell \mid \ell = 1, \dots, 80\}$ be the persistence diagrams of the atomic configurations sorted by the increasing order of temperatures (see [20, 25] for details). Figure 10 shows the KFDR graph of the PWGK. It should be noted that the problem size of this example is too big for the PSSK to have reasonable computational time, and hence we cannot obtain the KFDR for the PSSK. The maximum of the graph is given by $\ell = 39$, which corresponds to the temperature 3100K. In this example, the interval constructed by the standard method mentioned above is roughly estimated by [2000K, 3500K]. Therefore, we can conclude that our method statistically determines the glass transition tempera-

ture consistent to the conventional method.



Figure 10: The KFDR graph (left) and the Gram matrix (right) of the PWGK.

Figure 11 shows the 2-dimensional KPCA plot. Similar to the granular packings, the clear difference can be seen between before (red) and after (blue) the change point. This implies that the glass transition occurs at the detected change point.

5 Conclusion

In this paper, we have proposed the persistence weighted Gaussian kernel on persistence diagrams. As an significant advantage, our kernel enables one to control the effect of persistence in data analysis. We have also proved the stability results with respect to the kernel distance. Furthermore, we have analyzed the synthesized and real data by statistical methods based on the proposed kernel. For the granular packing and SiO_2 , the change point detection and the principal component analysis using the PWGK derived meaningful results in physics. From the viewpoint of computations, our kernel provides an accurate and efficient approximation to compute the Gram matrix, suitable for practical applications of TDA.

The statistical methods used in this paper are all unsupervised learning and all the parameters of our kernel are determined by the heuristic approach. In the future work, it will be of great importance to introduce a framework for tuning those parameters by supervised learning. Such a framework will further

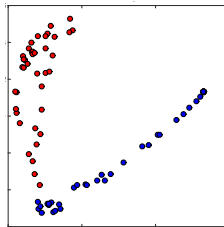


Figure 11: The KPCA plot of the PWGK.

emphasizes the advantage of our method including the flexibility and respecting the persistence.

Acknowledgement

We thank Mohammad Saadatfar and Takenobu Nakamura for providing experimental and simulation data used in Section 4.3 and 4.4. This work is partially supported by JST Mathematics CREST (15656429) and JSPS KAKENHI Grant Number 26540016.

References

- [1] Anonymous. What Is Random Packing?. *Nature*, 239, 488–489, 1972.
- [2] P. Bubenik. Statistical Topological Data Analysis using Persistence Landscapes. *Journal of Machine Learning Research*, 16, 77–102, 2015.
- [3] G. Carlsson. Topology and Data. *Bull. AMS.*, 46(2), 255–308, 2009.
- [4] G. Carlsson, T. Ishkhanov, V. de Silva and A. Zomorodian. On the local behavior of spaces of natural images. *Internat. J. Comput., Vision*, 76, 1–12, 2008.
- [5] CGAL webpage: <http://www.cgal.org/>
- [6] F. Chazal, V. de Silva, and S. Oudot. Persistence stability for geometric complexes. *Geometriae Dedicata*, 173, 193–214, 2014.
- [7] S. Chepushtanova, T. Emerson, E. Hanson, M. Kirby, F. Motta, R. Neville, C. Peterson, P. Shipman, and L. Ziegelmeier. Persistence Images: An Alternative Persistent Homology Representation. arXiv: 1507.06217.
- [8] D. Cohen-Steiner, H. Edelsbrunner, and J. Harer. Stability of Persistence Diagrams. *Discrete. Comput. Geom.*, 37(1), 103–120, 2007.
- [9] D. Cohen-Steiner, H. Edelsbrunner, J. Harer, and Y. Mileyko. Lipschitz Functions Have L_p -Stable Persistence. *Found. Comput. Math.*, 10, 127–139, 2010.
- [10] V. de Silva and R. Ghrist. Coverage in sensor networks via persistent homology. *Algebraic & Geometric Topology*, 7, 339–358, 2007.
- [11] J. Diestel and J. J. Uhl. *Vector Measures*. AMS. 1977.
- [12] H. Edelsbrunner. Persistent Homology in Image Processing. In *Graph-Based Representations in Pattern Recognition, Lecture Notes in Computer Science*, 7877, 182–183, 2013.
- [13] H. Edelsbrunner, D. Letscher, and A. Zomorodian. Topological persistence and simplification. *Discrete. Comput. Geom.*, 28, 511–533, 2002.

- [14] S. R. Elliott. *Physics of Amorphous Materials* (2nd ed). Longman, 1990.
- [15] B. T. Fasy, F. Lecci, A. Rinaldo, L. Wasserman, S. Balakrishnan, and A. Singh. Confidence sets for persistence diagrams. *Ann. Statist.*, 42(6), 2301–2339, 2014.
- [16] N. Francois, M. Saadatfar, R. Cruikshank, and A. Sheppard. Geometrical Frustration in Amorphous and Partially Crystallized Packings of Spheres. *Phys. Rev. Lett.*, 111, 148001, 2013.
- [17] M. Gameiro, Y. Hiraoka, S. Izumi, M. Kramar, K. Mischaikow, and V. Nanda. Topological Measurement of Protein Compressibility via Persistent Diagrams. *J. Indust. Appl. Math.*, 32, 1–17, 2015.
- [18] A. Gretton, K. Fukumizu, C. H. Teo, L. Song, B. Schölkopf, and A. Smola. A kernel statistical test of independence. *Advances in NIPS 20*, 585–592, MIT press, 2008.
- [19] Z. Harchaoui, F. Bach, and E. Moulines. Kernel change point analysis. In *Neural Information Processing Systems*, 21, 609–616, 2009.
- [20] Y. Hiraoka, T. Nakamura, A. Hirata, E. G. Escolar, K. Matsue, and Y. Nishiura. Hierarchical structures of amorphous solids characterized by persistent homology. arXiv: 1501.03611.
- [21] P. M. Kasson, A. Zomorodian, S. Park, N. Singhal, L. J. Guibas, and V. S. Pande. Persistent voids: a new structural metric for membrane fusion. *Bioinformatics*, 23(14), 1753–1759, 2007.
- [22] H. Lee, M. K. Chung, H. Kang, B. N. Kim, and D. S. Lee. Discriminative persistent homology of brain networks. *IEEE International Symposium on Biomedical Imaging*, 841–844, 2011.
- [23] K. Muandet, K. Fukumizu, F. Dinuzzo, and B. Schölkopf. Learning from Distributions via Support Measure Machines. *Advances in NIPS 26*, 10–18, 2012.
- [24] J. R. Munkres. *Elements of Algebraic Topology*. Westview Press, 1984.
- [25] T. Nakamura, Y. Hiraoka, A. Hirata, E. G. Escolar, and Y. Nishiura. Persistent Homology and Many-Body Atomic Structure for Medium-Range Order in the Glass. *Nanotechnology*, 26, 304001, 2015.
- [26] PHAT webpage: <https://code.google.com/p/phant/>
- [27] G. Petri, P. Expert, F. Turkheimer, R. Carhart-Harris, D. Nutt, P. J. Hellyer, and F. Vaccarino. Homological scaffolds of brain functional networks. *J. R. Soc. Interface*, 11, 20140873, 2014.

- [28] J. Reininghaus, S. Huber, U. Bauer, and R. Kwitt. A Stable Multi-Scale Kernel for Topological Machine Learning. Proc. 2015 IEEE Conf. Comp. Vision & Pat. Rec., 4741–4748, 2015.
- [29] A. Rahimi and B. Recht. Random Features for Large-Scale Kernel Machines. Advances in NIPS 20, 1177–1184, 2008.
- [30] V. Robins and K. Turner. Principal Component Analysis of Persistent Homology Rank Functions with case studies of Spatial Point Patterns, Sphere Packing and Colloids. arXiv: 1507.01454.
- [31] B. Schölkopf and A. J. Smola. Learning with Kernels. MIT Press, 2001.
- [32] G. Singh, F. Memoli, R. Ishkhanov, G. Sapiro, G. Carlsson, and D. L. Ringach. Topological analysis of population activity in visual cortex. Journal of vision, 8(8), 2008.
- [33] A. Smola, A. Gretton, L. Song, and B. Schölkopf. A Hilbert Space Embedding for Distributions. Algorithmic Learning Theory. Lecture Notes in Computer Sciences 4754, 13–31, Springer, 2007.
- [34] B. K. Sriperumbudur, K. Fukumizu, and G. R. G. Lanckriet. Universality, characteristic kernels and RKHS embedding of measures. Journal of Machine Learning Research, 12, 2389–2410, 2011.
- [35] B. Schölkopf, A. Smola, and K. Müller. Nonlinear Component Analysis as a Kernel Eigenvalue Problem. Neural Computation 10, 1299–1319, 1998.
- [36] H. Takeuchi, V. Robins, N. Francois, Y. Hiraoka, and M. Saadatfar. Topological description of granular crystallization. In preparation.
- [37] S. Torquato, T. M. Truskett, and P. G. Debenedetti. Is Random Close Packing of Spheres Well Defined?. Phys. Rev. Lett., 84, 2064–2067, 2000.
- [38] K. Xia, and G. W. Wei. Persistent homology analysis of protein structure, flexibility, and folding. Int. J. Numer. Meth. Biomed. Engng., 30, 814–844. 2014.

A Total persistence

In order to estimate constants L appearing in Section 3.2, especially show that the constant in Theorem 3.2 is independent of X and Y , we will review several properties of persistence.

Let (M, d_M) be a triangulable compact metric space. For a Lipschitz function $f : M \rightarrow \mathbb{R}$, the *degree- p total persistence* is defined by

$$\text{Pers}_p(f, t) = \sum_{\substack{x \in D_q(f) \\ \text{pers}(x) > t}} \text{pers}(x)^p$$

for $0 \leq t \leq \text{Amp}(f)$. Here, $\text{Amp}(f) := \max_{\mathbf{x} \in M} f(\mathbf{x}) - \min_{\mathbf{x} \in M} f(\mathbf{x})$ is the amplitude of f . Let K be a triangulated simplicial complex of M by a homeomorphism $\theta : |K| \rightarrow M$. The diameter of a simplex $\sigma \in K$ and the mesh of the triangulation K are defined by $\text{diam}(\sigma) = \max_{\mathbf{x}, \mathbf{y} \in \sigma} d_M(\theta(\mathbf{x}), \theta(\mathbf{y}))$ and $\text{mesh}(K) = \max_{\sigma \in K} \text{diam}(\sigma)$, respectively. Furthermore, let us set $N(r) = \min_{\text{mesh}(K) \leq r} \text{card}(K)$. The degree- p total persistence is bounded as follows:

Lemma A.1 (Cohen-Steiner et al. [9]). *Let M be a triangulable compact metric space and $f : M \rightarrow \mathbb{R}$ be a tame Lipschitz function. Then $\text{Pers}_p(f, t)$ is bounded from above by*

$$t^p N(t/\text{Lip}(f)) + p \int_{\varepsilon=t}^{\text{Amp}(f)} N(\varepsilon/\text{Lip}(f)) \varepsilon^{p-1} d\varepsilon,$$

where $\text{Lip}(f)$ is the Lipschitz constant of f .

For a compact subspace M in \mathbb{R}^d , the number of d -cubes with length $r > 0$ covering M is bounded for every $r > 0$. The minimum of these numbers is $N(r)$ and bounded from above by C_M/r^d for some constant C_M depending only on M .

For $p > d$, we can find upper bounds for the both terms as follows:

$$t^p N(t/\text{Lip}(f)) \leq t^p C_M \frac{\text{Lip}(f)^d}{t^d}$$

and

$$p \int_{\varepsilon=t}^{\text{Amp}(f)} N(\varepsilon/\text{Lip}(f)) \varepsilon^{p-1} d\varepsilon \leq \frac{p}{p-d} C_M \text{Lip}(f)^d \text{Amp}(f)^{p-d}.$$

We note $\lim_{t \rightarrow 0} t^p N(t/\text{Lip}(f)) = 0$ for $p > d$. Then, an upper bound of the total persistence $\text{Pers}(f) := \text{Pers}_p(f, 0)$ is given as follows:

Lemma A.2. *Let M be a triangulable compact subspace in \mathbb{R}^d and $p > d$. For any Lipschitz function $f : M \rightarrow \mathbb{R}$,*

$$\text{Pers}_p(f) \leq \frac{p}{p-d} C_M \text{Lip}(f)^d \text{Amp}(f)^{p-d},$$

where C_M is a constant depending only on M .

In the case of f_X , since X is a finite subset in \mathbb{R}^d , there exists an R -ball M containing X for some $R > 0$, which is a triangulable compact subspace in \mathbb{R}^d .

Lemma A.3. *Let M be a triangulable compact subspace in \mathbb{R}^d , $X = \{\mathbf{x}_1, \dots, \mathbf{x}_n\}$ be a finite subset of M , and $p > d$. Then*

$$\text{Pers}_p(f_X) \leq \frac{p}{p-d} C_M \text{diam}(M)^{p-d},$$

where C_M is a constant depending only on M .

Proof. The Lipschitz constant of f_X is 1, because, for any $\mathbf{x}, \mathbf{y} \in M$,

$$\begin{aligned} f_X(\mathbf{x}) - f_X(\mathbf{y}) &= \min_{\mathbf{x}_i \in X} d(\mathbf{x}, \mathbf{x}_i) - \min_{\mathbf{x}_i \in X} d(\mathbf{y}, \mathbf{x}_i) \\ &\leq \min_{\mathbf{x}_i \in X} (d(\mathbf{x}, \mathbf{y}) + d(\mathbf{y}, \mathbf{x}_i)) - \min_{\mathbf{x}_i \in X} d(\mathbf{y}, \mathbf{x}_i) \\ &= d(\mathbf{x}, \mathbf{y}). \end{aligned}$$

Moreover, the amplitude $\text{Amp}(f_X)$ is less than or equal to $\text{diam}(M)$, because $\min_{\mathbf{x} \in M} f_X(\mathbf{x}) = 0$ and $\max_{\mathbf{x} \in M} f_X(\mathbf{x}) \leq \text{diam}(M)$. \square

For more general, for a persistence diagram D , we define p -degree total persistence of D by $\text{Pers}_p(D) := \sum_{x \in D} \text{pers}(x)^p$. Let x_1, \dots, x_n be points of \underline{D} . Then we can consider the following n -dimensional vector from D :

$$v(D) := (\text{pers}(x_1), \dots, \text{pers}(x_n)).$$

Since each $\text{pers}(x)$ ($x \in \underline{D}$) is always positive, by using the ℓ^p -norm of $v(D)$, we have $\text{Pers}_p(D) = \|v(D)\|_p^p$. In general, since $\|v\|_q \leq \|v\|_p$ ($v \in \mathbb{R}^n$, $1 \leq p \leq q$), we have

$$\text{Pers}_q(D)^{\frac{1}{q}} = \|v(D)\|_q \leq \|v(D)\|_p = \text{Pers}_p(D)^{\frac{1}{p}}.$$

Proposition A.4. *If $1 \leq p \leq q < \infty$ and $\text{Pers}_p(D)$ is bounded, $\text{Pers}_q(D)$ is also bounded.*

B Proofs of Theorem 3.1 and Theorem 3.2

In fact, we can calculate the constant $L(f, g; C, p, \sigma)$ in Theorem 3.1 such as

$$\left\{ \frac{\sqrt{2}}{\sigma} \text{Pers}_p(D_q(f)) + 2p \text{Pers}_{p-1}(D_q(f)) + (2p+1) \text{Pers}_{p-1}(D_q(g)) \right\} C.$$

To obtain this value, we show several lemmas.

Lemma B.1. *For any $x, y \in \mathbb{R}^2$, $\|k_G(\cdot, x) - k_G(\cdot, y)\|_{\mathcal{H}_{k_G}} \leq \frac{\sqrt{2}}{\sigma} \|x - y\|_\infty$.*

Proof.

$$\begin{aligned} \|k_G(\cdot, x) - k_G(\cdot, y)\|_{\mathcal{H}_{k_G}}^2 &= k_G(x, x) + k_G(y, y) - 2k_G(x, y) \\ &= 1 + 1 - 2e^{-\frac{\|x-y\|^2}{2\sigma^2}} \\ &= 2 \left(1 - e^{-\frac{\|x-y\|^2}{2\sigma^2}} \right) \\ &\leq \frac{1}{\sigma^2} \|x - y\|^2 \tag{3} \end{aligned}$$

$$\leq \frac{2}{\sigma^2} \|x - y\|_\infty^2. \tag{4}$$

We have used the fact $1 - e^{-t} \leq t$ ($t \in \mathbb{R}$) in (3) and $\|x\|^2 \leq 2\|x\|_\infty^2$ ($x \in \mathbb{R}^2$) in (4). \square

Lemma B.2. For any $x, y \in \mathbb{R}^2$, the difference of persistences $|\text{pers}(x) - \text{pers}(y)|$ is less than or equal to $2 \|x - y\|_\infty$.

Proof. For $x = (x_1, x_2), y = (y_1, y_2)$, we have

$$\begin{aligned} |\text{pers}(x) - \text{pers}(y)| &= |(x_2 - x_1) - (y_2 - y_1)| \\ &\leq |x_2 - y_2| + |x_1 - y_1| \\ &\leq 2 \|x - y\|_\infty. \end{aligned}$$

□

Lemma B.3. For any $x, y \in \mathbb{R}^2$, we have

$$|w(x) - w(y)| \leq 2pC \max\{\text{pers}(x)^{p-1}, \text{pers}(y)^{p-1}\} \|x - y\|_\infty.$$

Proof.

$$\begin{aligned} |w(x) - w(y)| &= |\arctan(C\text{pers}(x)^p) - \arctan(C\text{pers}(y)^p)| \end{aligned} \quad (5)$$

$$\begin{aligned} &\leq C |\text{pers}(x)^p - \text{pers}(y)^p| \\ &\leq C |\text{pers}(x) - \text{pers}(y)| p \max\{\text{pers}(x)^{p-1}, \text{pers}(y)^{p-1}\} \\ &\leq 2pC \max\{\text{pers}(x)^{p-1}, \text{pers}(y)^{p-1}\} \|x - y\|_\infty. \end{aligned} \quad (6)$$

We have used the fact that the Lipschitz constant of \arctan is 1 in (5) and for any $s, t \in \mathbb{R}$,

$$\begin{aligned} s^p - t^p &= (s - t)(s^{p-1} + s^{p-2}t + \dots + t^{p-1}) \\ &\leq (s - t)p \max\{s^{p-1}, t^{p-1}\} \end{aligned}$$

in (6). □

Theorem 3.1 is a stability result for functions $f, g : M \rightarrow \mathbb{R}$. If $\|f - g\|_\infty < \varepsilon$, from Proposition 2.1, the bottleneck distance $d_B(D_q(f), D_q(g))$ is less than ε . From now on, we show a generalized stability result. That is, for two finite persistence diagrams D and E satisfying $d_B(D, E) < \varepsilon$, we will find a constant L such that

$$d_{k_G}^w(D, E) < L\varepsilon.$$

Here, let a multi-bijection $\gamma : D \rightarrow E$ such that $\sup_{x \in D} \|x - \gamma(x)\|_\infty < \varepsilon$ and $E' := \underline{E} - (\gamma(\underline{D}) - \Delta)$. By the definition of γ , each point in E' is ε -close to the diagonal.

$$\begin{aligned}
& d_{k_G}^w(D, E) \\
&= \left\| \int k_G(\cdot, x) d\mu_D^w(x) - \int k_G(\cdot, x) d\mu_E^w(y) \right\|_{\mathcal{H}_{k_G}} \\
&= \left\| \int k_G(\cdot, x) d\mu_D^w(x) - \int k_G(\cdot, y) d\mu_{\gamma(D)}^w(y) - \int k_G(\cdot, y) d\mu_{E'}^w(y) \right\|_{\mathcal{H}_{k_G}} \\
&= \left\| \sum_{x \in D} w(x) k_G(\cdot, x) - \sum_{x \in D} w(\gamma(x)) k_G(\cdot, \gamma(x)) - \sum_{y \in E'} w(y) k_G(\cdot, y) \right\|_{\mathcal{H}_{k_G}} \\
&\leq \left\| \sum_{x \in D} w(x) k_G(\cdot, x) - \sum_{x \in D} w(x) k_G(\cdot, \gamma(x)) \right\|_{\mathcal{H}_{k_G}} \\
&\quad + \left\| \sum_{x \in D} w(x) k_G(\cdot, \gamma(x)) - \sum_{x \in D} w(\gamma(x)) k_G(\cdot, \gamma(x)) \right\|_{\mathcal{H}_{k_G}} + \left\| \sum_{y \in E'} w(y) k_G(\cdot, y) \right\|_{\mathcal{H}_{k_G}} \\
&\leq \sum_{x \in D} w(x) \|k_G(\cdot, x) - k_G(\cdot, \gamma(x))\|_{\mathcal{H}_{k_G}} + \sum_{x \in D} |w(x) - w(\gamma(x))| \|k_G(\cdot, \gamma(x))\|_{\mathcal{H}_{k_G}} \\
&\quad + \sum_{y \in E'} w(y) \|k_G(\cdot, y)\|_{\mathcal{H}_{k_G}} \tag{7}
\end{aligned}$$

Form Lemma B.1, we have

$$\|k_G(\cdot, x) - k_G(\cdot, \gamma(x))\|_{\mathcal{H}_{k_G}} \leq \frac{\sqrt{2}}{\sigma} \|x - \gamma(x)\|_{\infty},$$

from Lemma B.3,

$$|w(x) - w(\gamma(x))| \leq 2pC \max\{\text{pers}(x)^{p-1}, \text{pers}(\gamma(x))^{p-1}\} \|x - \gamma(x)\|_{\infty}.$$

Moreover, for any $x \in \mathbb{R}^2$ we have $\|k_G(\cdot, x)\|_{\mathcal{H}_{k_G}} = \sqrt{k_G(x, x)} = 1$. Therefore,

the continuation of (7) is

$$\begin{aligned}
& \sum_{x \in D} w(x) \frac{\sqrt{2}}{\sigma} \|x - \gamma(x)\|_\infty \\
& + \sum_{x \in D} 2pC \max\{\text{pers}(x)^{p-1}, \text{pers}(\gamma(x))^{p-1}\} \|x - \gamma(x)\|_\infty + \sum_{y \in E'} w(y) \\
& \leq \frac{\sqrt{2}}{\sigma} C\varepsilon \sum_{x \in D} \text{pers}(x)^p + 2pC\varepsilon \sum_{x \in D} (\text{pers}(x)^{p-1} + \text{pers}(\gamma(x))^{p-1}) + C \sum_{y \in E'} \text{pers}(y)^p \\
& \leq \frac{\sqrt{2}}{\sigma} C\varepsilon \sum_{x \in D} \text{pers}(x)^p + 2pC\varepsilon \sum_{x \in D} (\text{pers}(x)^{p-1} + \text{pers}(\gamma(x))^{p-1}) + C\varepsilon \sum_{y \in E'} \text{pers}(y)^{p-1} \tag{8}
\end{aligned}$$

$$= \left\{ \frac{\sqrt{2}}{\sigma} \text{Pers}_p(D) + 2p(\text{Pers}_{p-1}(D) + \text{Pers}_{p-1}(\gamma(D))) + \text{Pers}_{p-1}(E') \right\} C\varepsilon \tag{9}$$

$$= \left\{ \frac{\sqrt{2}}{\sigma} \text{Pers}_p(D) + 2p\text{Pers}_{p-1}(D) + (2p+1)\text{Pers}_{p-1}(E) \right\} C\varepsilon. \tag{10}$$

We have used the fact $\text{pers}(y) \leq \varepsilon$ ($y \in E'$) in (8) and $\text{Pers}_{p-1}(\gamma(D)), \text{Pers}_{p-1}(E') \leq \text{Pers}_{p-1}(E)$ in (10). Thus, if both $(p-1)$ -degree total persistence of D and that of E are bounded, since p -degree total persistence of D is also bounded from Proposition A.4, the coefficient of ε appearing in (10) is bounded.

Proof of Theorem 3.1. From Lemma A.2, for any Lipschitz function $f : M \rightarrow \mathbb{R}$, there exists a constant $C_M > 0$ such that

$$\text{Pers}_{p-1}(f) \leq \frac{p-1}{p-1-d} C_M \text{Lip}(f)^d \text{Amp}(f)^{p-1-d}.$$

Since M is compact, $\text{Amp}(f)$ is bounded, and hence $\text{Pers}_{p-1}(f)$ is bounded. Replacing D and E with $D_q(f)$ and $D_q(g)$ in (10), respectively, we have

$$L(f, g; C, p, \sigma) = \left\{ \frac{\sqrt{2}}{\sigma} \text{Pers}_p(f) + 2p\text{Pers}_{p-1}(f) + (2p+1)\text{Pers}_{p-1}(g) \right\} C.$$

□

Proof of Theorem 3.2. For any point set $X \subset M$, from Lemma A.3, there exists a constant $C_M > 0$ such that

$$\text{Pers}_p(D_q(X)) \leq \frac{p}{p-d} C_M \text{diam}(M)^{p-d}.$$

Thus, we have the continuation of (10) as follows:

$$\begin{aligned}
& \frac{\sqrt{2}}{\sigma} \text{Pers}_p(D_q(X)) + 2p \text{Pers}_{p-1}(D_q(X)) + (2p+1) \text{Pers}_{p-1}(D_q(Y)) \\
& \leq \frac{\sqrt{2}}{\sigma} \frac{p}{p-d} C_M \text{diam}(M)^{p-d} + (4p+1) \frac{p-1}{p-1-d} C_M \text{diam}(M)^{p-1-d} \\
& = L(M, d; C, p, \sigma).
\end{aligned}$$

This value is a constant dependent on M, d, C, p, σ but independent of X, Y . \square